University of Bristol - Explore Bristol Research
General rights

AUXHEX – a Kirigami inspired Zero Poisson Ratio cellular structure

Simone Del Broccolo[1, 2], Susanna Laurenzi[1], Fabrizio Scarpa[2*]

[1]Department of Astronautic, Electrical and Energy Engineering, Sapienza University of Rome, Via Salaria 851-881, 00138 Rome, Italy

[2]Advanced Composites Centre for Innovation and Science (ACCIS), University of Bristol, BS81TR Bristol, UK

Abstract

This work describes the development, manufacturing and testing of a zero Poisson's ratio PEEK cellular structure (AuxHex) made using Kirigami-inspired techniques. The AuxHex hybrid cell pattern is a combination of cells with different shapes that interlock with each other. This principle can lead to graded honeycombs possessing, in different areas, synclastic as well as anticlastic behavior. The AuxHex samples produced have been tested for flatwise compression according to ASTM standards and the results are compared with a unit-cell-based analytical model. Hexagonal-cell shaped honeycombs were also produced with the same technique and used for direct comparison. The mechanical flatwise properties have been benchmarked against the ones of other experimental PEEK-based cores and commercially available honeycombs. AuxHex samples are found to have higher stiffness compared to other experimental PEEK honeycombs, but lower compared with the commercially available honeycombs. The strength thought, while it is still higher compared to the other experimental PEEK cores, it is comparable with other honeycomb configurations.

Keywords: Honeycomb, Kirigami, Zero Poisson's ratio, thermoplastics, flatwise compression.

*Corresponding author.   E-mail address: f.scarpa@bristol.ac.uk (Fabrizio Scarpa)

1. Introduction

Morphing and deployable aerospace structures exploit the principle of mass and mechanical efficiency, as they remove the burden of implementing heavy actuating systems and joints in the design of the airframe. Futuristic morphing wings [1-4] for the aviation industry or deployable structures like solar panels [5-9], antennas or inflatable modules for to the International Space Station (ISS) are becoming reality. The Bigelow Expandable Activity Module (BEAM) [10] represents the first deployable/inflatable pressurized module attached to the ISS. Almost all satellites that mount equipment with large energy requirements do have deployable solar panels. Cellular cores are very attractive for such purposes and different manufacturing techniques can be used to produce panels depending on its constituent material, as well as its cell shape. Some of those are based on gluing or soldering in precise locations strips of material that are then pulled apart, creating a three dimensional cellular structure. Another option is to pile up a large number of corrugated sheets and consequently join them together with the above-mentioned intrusive methods. Between the most innovative techniques used to produce honeycombs is the Kirigami-inspired one. Kirigami is a variation of Origami, an ancient Japanese technique that consists in creating 3D structures by folding a 2D sheet of material. Origami only allows folding, while Kirigami includes sharp cut slits and, if needed, material removal. Saito and Nojima developed the Kirigami-inspired technique [11] for the manufacturing of honeycombs. Since the publication of their seminal paper they have applied the Kirigami technique to create various types of cellular solids [12, 13] and deployable structures [14, 15]. In the aerospace field, Saito and co-authors have also designed and manufactured an autoclave cured woven Kevlar cellular wing box using Kirigami[16]. Neville and Scarpa exploited this technique to

create morphing open cell honeycombs, including embedded actuating cables [17, 18]. Saito et al [19] have also developed a mathematical tool that creates Kirigami cutting/folding line diagrams for honeycombs that require complex curvatures, without any machining and therefore, material waste. The Jet Propulsion Laboratory (JPL) is working on Origami/Kirigami inspired deployable solar panels [20] and, using flexible solar cells, Lamoureux and co-authors produced a prototypal dynamic Kirigami solar panel with integrated solar tracking [21]. Applications of this cutting and folding technique has been applied to electrically conductive composite materials, increasing their strain from about 5% to 370%, without significantly affecting their conductivity. The design strategy adopted by Shyu and Kotov is to combine a strong elastic material, with another one that possesse the desired electrical conductivity [22]. A similar application of Kirigami has been also studied by Blees with graphene sheets, which are known to stretch very little [23]. The tools and materials used so far for engineering applications of Kirigami are very diverse. Materials go from paper, thin metallic sheets, graphene, thermoplastics, elastomers, and composite materials like carbon fiber reinforced plastics (CFRP) or aramid paper (Kevlar fibers)[24]. Morphing structures require materials able to follow the change in shape in one direction possibly with no consequences in the orthogonal plane. The index that describes this type of characteristic is the Poisson's ratio, explained in Fig. 1. This can be positive, which means material will expand in the two perpendicular directions in respect to the direction of compression and vice versa, negative (NPR and auxetic) which will have its cross-section reduced, perpendicularly to the direction of compression, and zero (ZPR) which satisfies the morphing structure requirements. .

Zero Poisson ratio (ZPR) cellular structures have no synclastic or anticlastic behavior, as Grima and co-authors show in their work [25]. With such ZPR core panels it would be possible to follow axial curvatures and build lightweight, cylindrical structures.

This work is focused on the development of a ZPR-PEEK adhesive less honeycomb called the AUXHEX, which is obtained by using a Kirigami-inspired manufacturing technique. Classic hexagonal shaped honeycombs have also been produce with the same material substrate for comparative reasons. PEEK is a semi-crystalline engineering thermoplastic polymer widely used in different fields such as aerospace, automotive, medical, energy and electronics industries. PEEK combines distinguishing mechanical properties and excellent chemical resistance but, mostly, it can be used within a very wide temperature range compared to other plastics, starting from -60°C up to 260°C. The combination of material and manufacturing technique has allowed us to include in the process steps like the creation of venting holes for panel space application. For both the novel ZPR and the hexagonal honeycomb configurations flatwise compression tests have been carried out according to ASTM C365 standard. The results have been compared with the ones from an analytical model produced for the AuxHex configuration, as well as the classic hexagonal topology. Finally, the AuxHex flatwise mechanical properties have been compared with commercially available cores found on the market.

2. Geometry and analytical model

2.1 The AuxHex geometry

Kirigami allows the creation of honeycombs with cells of different shape. In order to obtain a regular tessellated Kirigami honeycomb, one must guarantee that the cell cross section has two parallel sides of the same dimensions. Those sides should face each

other once the sheet is folded back. Polygonal cross sections such as trapeziums, rectangles, squares, parallelograms and rhombus, are all compatible with Kirigami. By combining these shapes, many different cell geometries and patterns of mixed cells are obtainable. The proposed AuxHex configuration, shown in Fig. 2, is characterized by a ZPR behavior within the plane. It is composed of three different types of cells: an hexagonal, a re-entrant (butterfly) and a semi re-entrant (arrow). To give a demonstration of the zero Poisson's ratio effect we have carried out a linear static Finite Element analysis using the ABAQUS 6.14 code. The simulation represents an in-plane uniaxial compression (small axial displacement of 2mm) of a lattice configuration made in steel and composed of deformable B31 beams. The honeycomb demonstrator is made of two rows, each containing two unit cells. The unit cell was discretized with 14 beams all linked with each other through hinges. The mesh is composed by 584 elements and 574 nodes..No stiffness is given to the hinges since the purpose of the simulation is only to demonstrate the ZPR behavior. The horizontal beams placed on the lower part of the bottom row of unit cells are clamped along the the three directions X,Y,Z. The in-plane compression is applied to the upper horizontal beams of the top cells row. If the structure has an equal number of positive, negative and zero Poisson ratio cells, the overall behavior of the honeycomb hybrid pattern is zero. Fig. 3 shows how a compression or traction along the Y direction causes the hinge distance in the X direction to be unchanged for the semi re-entrant cells, while the positive Poisson's ratio behavior of the hexagonal cells is completely compensated by the negative Poisson's ratio effect possessed by the re-entrant cells.

2.2 Analytical model

An analytical model for the prediction of the buckling strengths of both the hexagonal and the AuxHex configurations when loaded across the Z (compression) direction has been developed. The model follows a similar procedure to the one proposed by Gibson and Ashby [26] for honeycombs with hexagonal unit cells where the walls have all the same thickness. Kirigami-inspired and classic manufacturing techniques produce honeycombs with double walls in correspondence to the glued/soldered areas. Fig. 4 shows the representative the unit cell of the AuxHex configuration, from which the hexagonal unit for classic honeycombs can be derived. Fig. 5 shows how the unit cells can be considered made of a certain number of single walls of different sizes. Our model only considers the ultimate compressive strength, and it is based on the assumption that the single walls of the cell all buckle simultaneously. The assumption is considered to be reasonable since all the cell walls experience the same finite deflection before the honeycomb collapses. The critical buckling load for the single cell wall can be determined by the second moment of inertia of the wall itself and the wall width b:

$$P_{crit} = \frac{KEt^3}{b(1-v^2)} \qquad (1)$$

Where K is the end constraint factor, which is a value describing the degree of end fixity or constraint, E is the Young's modulus of the constituent material, t is the wall thickness and v is the Poisson's ratio. The AuxHex unit cells have walls of double thickness, therefore the corresponding critical buckling load is $8P_{crit}$. Depending on the position of the unit cell within the core panel one can find cells that are completely surrounded by other cells, and others, along the panel perimeter, that will not have the same constraints. For this reason, different end constraint factors K dependent from the

6

$^a/_b$ ratio are considered in the model. The values for K can be found in various literature sources [27]. The elastic collapse stress will therefore be the sum of the critical buckling load of each wall, divided by the cell total cross section. For the hexagonal and AuxHex part the cross sections can be calculated from Figure 4 as:

$$A_{cell}^{hex} = (2L \cos \vartheta) \cdot (2H + L) \qquad (2)$$
$$A_{cell}^{aux} = (2L \cos \vartheta) \cdot (2H + 4L) \qquad (3)$$

The in-plane unit cell cross section A_{cell}^{hex} is 166.28 mm² and A_{cell}^{aux} is 353.34 mm². Those results are obtained for ϑ=30°, L = 6 mm and H = 5mm.

Figure 5 shows how both the hexagonal and the re-entrant cells have walls of the same dimensions because the tool bar used to produce the cells with the Kirigami process has the same trapezoidal shape. The specific toolbar used imposes a ratio of 1.2 between L and H.

The values of the elastic collapse stress for all configurations and constraint factors considered are shown in Table 1. In this case all the walls are considered to have the same constraint factor. This is only a limiting assumption because a unit cell on the outer perimeter of the panel has both walls connected to the neighbor cells and free walls with adjacent cells. A calculation for a cell in the external perimeter (in the corner of the panel) is carried out to evaluate the differences that may result with a cell positioned in the center of the panel. Constraints described in Fig. 6 refer to the ones applied at the 'a' sides of the walls. The 'b' sides are considered as simply supported. With these assumptions, one can use the formula for the elastic collapse stress for any unit cell part of a cellular structure:

$$\sigma_z = \frac{\sum_{i=0}^{n} iP_{crit}^j}{A_{cell}} \qquad (4)$$

For PEEK films[28] the application of (4) leads to a buckling stress of 2.09 MPa, a value between the one calculated with the 'a' sides having all (SS/C) or (C/Free) constraints, suggesting that the real boundary conditions are somehow a hybrid version between these two.

The transverse Young's Modulus E_z in the Z direction is simply proportional to the modulus of the constituent bulk material E_s scaled by the area of the load-bearing section, which is directly proportional to the relative density:

$$E_z = \frac{\rho^*}{\rho} E_s \qquad (5)$$

The theoretical relative density that the samples should achieve after manufacturing is of 0.068 for the hexagonal configuration and 0.081 for the AuxHex. Consequently, the values of the Young's compression modulus calculated were 155.48MPa for the hexagonal configuration and 184.7MPa for the AuxHex one.

3. Manufacturing and test methods

The raw substrate selected for the manufacturing of the cellular cores is the PEEK Aptiv® 2000 series film with 250μm thickness[28]. The Kirigami-inspired technique consists in thermoforming a slotted and pierced sheet of PEEK using a modular mould, which consists in a steel plate and aluminum bars. Fig. 7 shows the bar arrangement in order to produce the AuxHex and the hexagonal cores. The starting point is therefore sizing the sheet of material and the slits needed to produce the samples. The sample height, the number of cells in each row and their geometry semi-perimeter directly influence the dimensions of the sheet used. Very neat cuts are also required by Kirigami procedures since they allow the accurate folding and are therefore an index of the overall quality of the sample. A computer numerical control (CNC) cutting machine

assured this requirement. Fig. 8 shows a full production cycle, from the cutting to the final manufacturing stage of a sample. The cross section of the mould bars is a crucial aspect as its the final cell shape of the structure (Fig. 9). Ventilation holes (Fig. 10b) are directly carved on the 2D sheet before the thermoforming process, using a very sharp drill with a diameter of 1 mm). The PEEK sheet is placed over and under the bars; the latter are kept tightly packed and fixed onto the steel plate with the aid of a heat resistant tape. The thermoforming process consists in pre-heating an oven above the PEEK's glass transition temperature of 143°C and then placing the mould inside for about an hour. This time is in general sufficient to guarantee that the mould would heat up above the polymer T_g since the oven is set at about 200°C. When the PEEK reaches and goes beyond its T_g temperature its color changes but most importantly becomes opaque, which makes the thermoforming cut-off point very easy to determine. The corrugated sheet obtained is then transformed into the 3D structure by folding it backwards and forward. PEEK is well known for its high chemical resistance; this makes it a very difficult plastic to join on itself. Cyanoacrylate as well as epoxy adhesives have been previously tested[29, 30], but the best option in our case consisted in join-melting where needed. By using a traditional gas soldering station the folded parts that were supposed to be glued to close the cells were molten and joined together (Fig. 10a), creating cellular structures with no additional material added. The manufactured samples are shown in Fig. 11 and their average volume, weight, density, together with surface section and effective surface area, are reported in Table 2.

3.1. Compressive tests

The compressive tests were performed according to the ASTM C365/C365Ms [31]. A 50kN Zwick tensile testing machine with a load cell of 50 KN has been used for the

flatwise compression test. The bottom platen, as well as the top platen, was checked for concentricity and the specimen area (specimen perimeter) was centered and marked using paper tape (Fig. 12). The specimen was placed in position and the top self-adjustable plate was brought in contact with the specimen, avoiding excessive preloading. The ASTM considers acceptable a 45N preloading before the test run. Such preloading guarantees that the sample lays perfectly flat onto the bottom platen and adjusts the top platen. The ASTM test speed is 0.5mm/min and should cause failure in 3-6 minutes. A trial run has been carried out using a 3D printed PLA dummy honeycomb of exactly the same geometry and dimensions. Tests were stopped when the displacement of the platen reached a value of 3.5 mm. The sampling frequency was set to 10Hz and values of load over displacement were recorded. The value of the ultimate strength is calculated as follows:

$$F_z^{fcu} = \frac{P_{max}}{A} \tag{6}$$

Where F_z^{fcu} is the ultimate flatwise compressive strength, P_{max} is the ultimate force prior to failure and finally, A is the cross sectional area. The strain values are also calculated with the following formula:

$$\varepsilon = \frac{\Delta L}{L} = \frac{L - l}{L} \tag{7}$$

Where L is the initial specimen height, l is the final specimen height and ΔL is the relative displacement. The compressive chord modulus E_z^{fc} is obtainable from the given equation which refers to load/displacement data:

$$E_z^{fc} = \frac{[(P_{0.003} - P_{0.001}) \cdot t]}{[(\delta_{0.003} - \delta_{0.001}) \cdot A]} \qquad (8)$$

Where $P_{0.003}$ is the applied force corresponding to $\delta_{0.003}$ and $P_{0.001}$ is the applied force corresponding to $\delta_{0.001}$. The delta values just mentioned are the recorded deflection values such that δ/t is closest to 0.003 and 0.001 respectively; t is the specimen height and A is the specimen surface area normal to the loading direction.

The value of the Young's modulus can be directly calculated from the stress/strain data. The calculation of the elastic modulus has been carried out taking into account possible take-up of slack and poor positioning of the specimen. All those contribute as an error in the initial testing stage. A toe compensation was necessary in order to properly restrain the calculation in the linear elastic region.

4. Results and discussions

A comparison between the mechanical results and the predicted values calculated through the analytical model has been performed and benchmarked against the specific properties of commercially available cores as well as with the ZPR Silicomb [29, 30, 32]. The ultimate force for the analytical model has been calculated knowing the theoretical surface area that a manufactured sample should have.

4.1. Ultimate compressive strength and Young's modulus

The analytical model boundary conditions assumed for both configurations included simply supports for all the walls of the unit-cell. The relative density of cellular structures is a primary metrics for the performance of these honeycomb solids. Keeping the number of cells fixed as well as the surface area normal to the loading direction and volume of the specimen, a higher relative core density either results in thicker cell walls

or in a larger cell perimeter. The AuxHex configuration has a higher theoretical core density compared to the Hexagonal shape. As shown on Fig. 13: UFig. 13 the experimental ultimate strength is higher for the hexagonal configuration than the one found for the AuxHex honeycomb, with average values of 2.1±0.16 MPa and 1.81±0.05 MPa respectively. The opposite result is obtained in the analytical model. In particular, the analytical compressive strength was 2.27 MPa for the hexagonal and 2.57 MPa for the AuxHex. The tailored boundary conditions used to simulate a unit cell placed on the peripheral area gave a result of 2.09 MPa, which is closer to the experimental results. The Young's modulus calculated using the analytical model is higher for the AuxHex configuration (184.7 MPa) with respect to the Hexagonal one (155.5 MPa), since the proportionality with the relative density is valid for this property as well. From the ASTM testing instead, this value is greater for the Hexagonal configuration (Fig. 14). Both experimental quantities (ultimate strength and Young's modulus) are in contrast with the analytical model. In addition, the Young's modulus estimated with the model for the Hexagonal configuration is five times greater than the one calculated experimentally. To make an effective comparison between honeycombs of different constituent materials and relative densities, it is necessary to normalize the properties of the cellular solids. For flatwise compression, the following identity has been used:

$$\frac{property/E_s}{\rho^*/\rho} \qquad (9)$$

Where E_s is the PEEK Young's modulus and ρ^*/ρ is the relative density of the cellular core. The properties that will be considered are the Young's modulus of the core and its ultimate strength, as shown in Table 3. Fig. 15**Error! Reference source not found.** to Fig. 18 show the comparison of the AuxHex configuration with the Silicomb one and with other types of commercial honeycombs listed in Table 4. These honeycombs differ

in cell size and type, relative density, and constituent material. From the Figures it is evident that the mechanical performance of the AuxHex honeycomb is superior to the Silicomb one, however both of them result to have lower specific stiffness and strength if compared with the commercial ones. In particular, the stiffness of the AuxHex is higher than the one of the Silicomb. It is however worth of notice that the strength of the AuxHex configuration is comparable with the one from commercial competitors.

The presence of the ventilation holes may also have contributed to the discrepancy between the model prediction and the mechanical testing. The effect is to create stress concentration points where failure could potentially initiate, lowering the bucking load. The diameter of the vent holes (1 mm) is small compared to the wall width (6 mm), therefore their contribution to lowering the stiffness is considered minor[33].

Onck et al. have shown that there is a connection between the relative cell size to the other dimensions of the honeycomb[34]. When the specimen size is comparable to the cell size, the specimen properties are significantly different from the bulk predicted properties of an infinite honeycomb. As the specimen size is increased, the specimen properties approach the bulk properties due to the proportion of the specimen material present in the peripheral area of the specimen, which contributes little to the modulus or strength of the honeycomb. The frame of the open cells around a specimen is made up of truncated closed cells; as such it must be less than one cell size in width, regardless of the specimen size. However, the inner portion of the specimen, which is constituted by closed cells, is proportional to the square of the specimen size, so as the specimen becomes bigger the closed cell properties dominate and the effect of the open cells becomes less significant. Foo[35] also shows that the out-of-plane modulus strongly depends on the number of cells present in the sample. Our specimens fulfilled the

ASTM sample dimensioning but they represented the largest possible specimen with the minimum amount of cells required. This probably made the effect of the truncated cell frame, as well as the low number of cells, to lower both the elastic modulus and the strength. For this reason, a calculation simulating the constraints of a cell placed in the peripheral area of the panel has been carried out through careful evaluation of the boundary condition of each wall. In this case, an open cell has walls with free edges, which significantly lowers its bucking load compared to a closed cell. The model that we follow [26, 36] considers the cell walls as plates undergoing Eulerian bucking. The bucking strength of the wall is determined in part by their aspect ratio through the value of the constant K, which is included in the calculation of the critical wall bucking load. The higher the aspect ratio, the lower is the value of K, which is directly proportional to the buckling load. Almost all the commercial honeycombs selected for the comparison resulted having approximately the same wall width but smaller height (15 mm vs 12.5 mm; a factor of 1.2) leading to lower values of K. The ultimate compressive strength of the commercial honeycombs calculated applying this model would lead to greater values of the ultimate compressive strength compared to the AuxHex core. This agrees well with the results obtained from the comparison between their datasheet values and the AuxHex experimental testing.

5. Conclusions

The AuxHex ZPR PEEK honeycomb seems to be a valid option for applications where a low density, non-metallic core is required. Comparing the AuxHex ZPR honeycomb with another PEEK ZPR honeycomb present in literature we observe that even if the value of their relative densities is very similar, the ultimate compressive strength of the AuxHex is more than twice the one of the Silicomb. Soldering the cells has produced

14

joints that resulted to hold much stronger than the epoxy ones. The analytical model adopted takes into consideration the double wall left behind during the folding process, and the strength predictions show in general good agreement with the mechanical testing results. The boundary conditions used in the model for the unit cell play a crucial role in terms of calculated mechanical properties. As we have tested bare honeycomb cores, the most reasonable boundary condition to be used in the model for all walls seemed to be the simply supported one.

The AuxHex configuration was predicted to have slightly greater ultimate compression strength with respect to the hexagonal honeycomb, and this data was found to disagree with the mechanical results probably because the AuxHex geometry is more complex to manufacture compared to the more classic hexagonal one. The consequent quality of the samples has impacted the results. The number of cells to surface area ratio in our samples made also the border effect to be noticeable. This would explain, together with the sample manufacturing quality, why the mechanical results are lower compared to the predicted values. A second calculation for the AuxHex unit cel using tailored boundary conditions made the value of the ultimate compressive stress closer to the mechanical testing results. The stiffness of the AuxHex and Hexagonal PEEK honeycomb is low compared to that of commercial counterparts, but its strength is comparable.
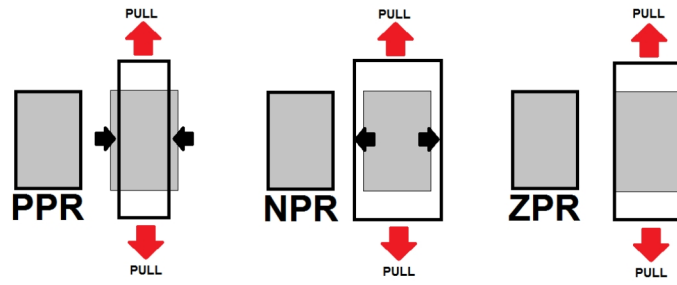
Figures

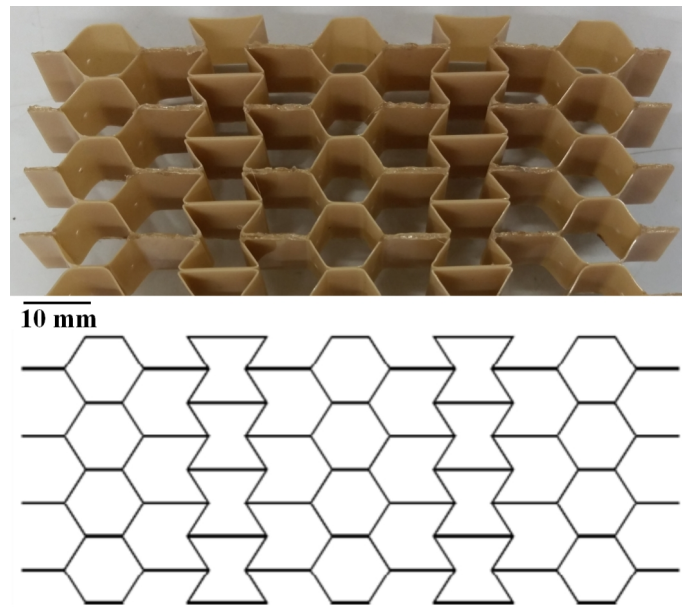Fig. 1: Two-dimension Poisson's ratio explained.

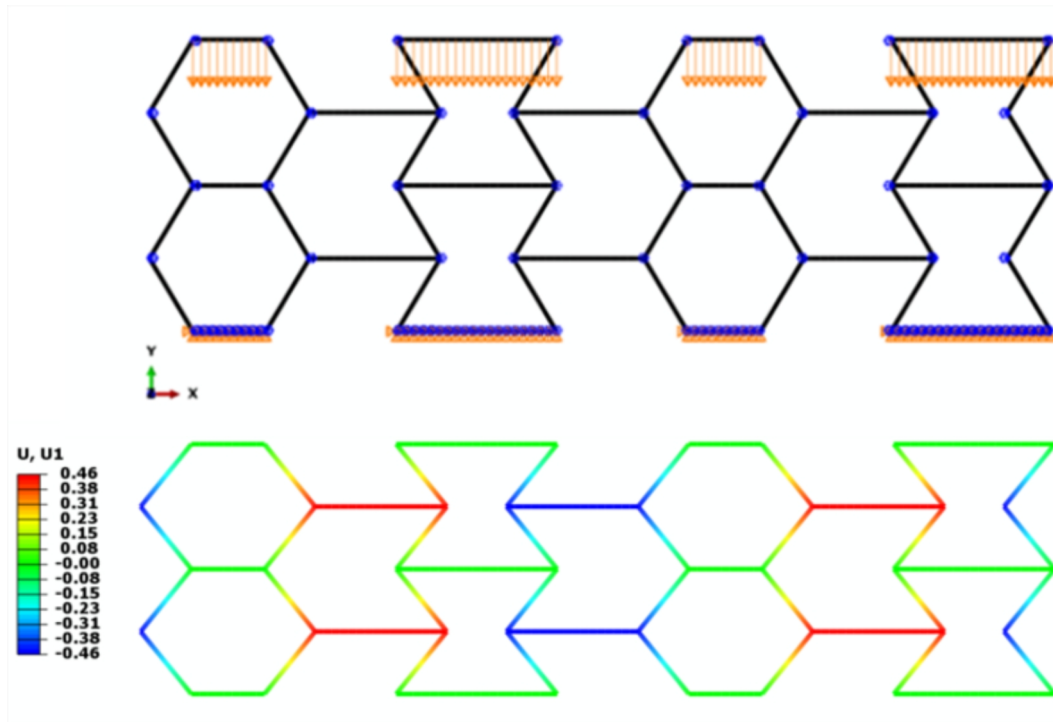Fig. 2: AUXHEX sample post-soldering process comparison with 2D pattern model.

Fig. 3: In-plane axial compression simulation of AuxHex geometry showing zero Poisson's ratio behavior. Non-deformed (top) and deformed shape (bottom).
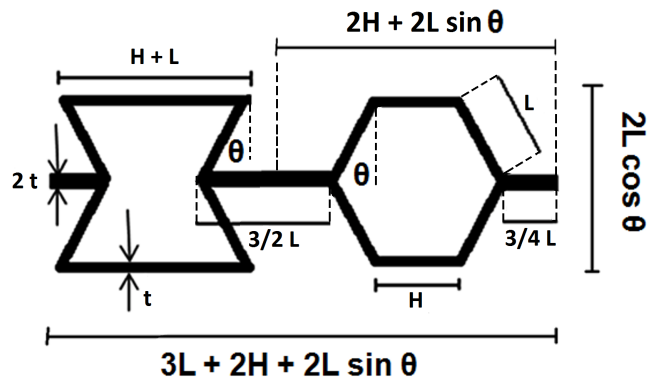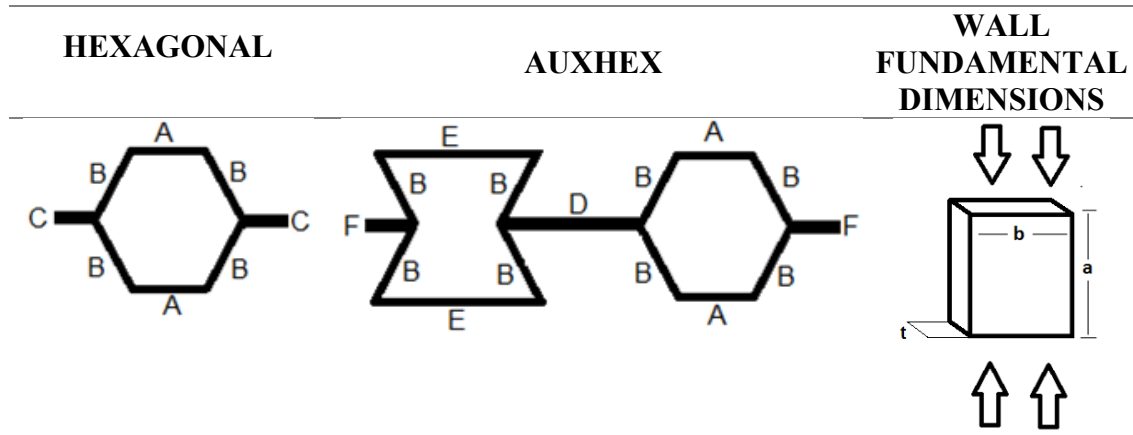

Fig. 4: AuxHex unit cell used for analytical model.

| HEXAGONAL | AUXHEX | WALL FUNDAMENTAL DIMENSIONS |

HEXAGONAL

WALL TYPE	a (mm)	b (mm)	t (mm)	Parameter
A	15.00	5.00	0.25	H
B	15.00	6.00	0.25	L
C	15.00	2.50	0.50	(1/2)H

AUXHEX

WALL TYPE	a (mm)	b (mm)	t (mm)	Parameter
A	15.00	5.00	0.25	H
B	15.00	6.00	0.25	L
D	15.00	9.00	0.50	(3/2)H
E	15.00	11.00	0.25	H + L
F	15.00	4.50	0.50	(3/4)H

Fig. 5: Unit cells for both configurations and wall type distinction.

AUXHEX CORNER UNIT CELL	WALL	CONSTRAINT
	A1	S/S
	A2	S/Free
	B1	S/C
	B2	S/C
	B3	S/S
	B4	S/S
	B5	S/C
	B6	S/S
	B7	S/S
	B8	S/S
	D1	S/S
	E1	S/C
	E2	S/S
	F1	C/C
	F2	S/S

Fig. 6: Tailored corner AuxHex unit cell showing boundary conditions for each wall.
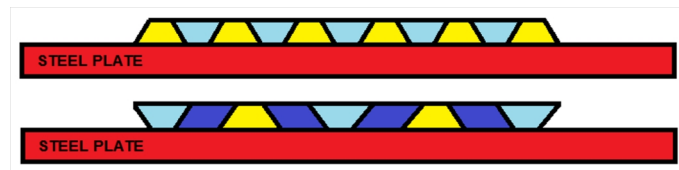
Fig. 7: Mould bars disposition for hexagonal (top) and AuxHex (bottom) configurations. The dark blue bars are the ones that will produce semi re-entrant ZPR cells.
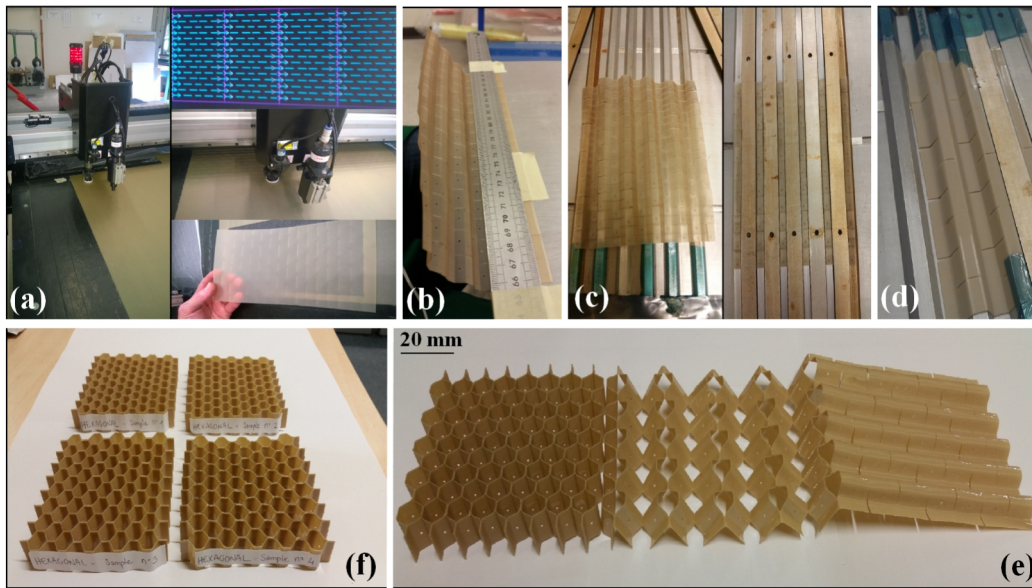
Fig. 8: Sequential steps of the manufacturing process: (a) CNC cutting; (b) pre-folding; (c) pre-folded PEEK closed in the mould ready for thermoforming; (d) thermoformed PEEK; (e) thermoformed sheet undergoing Kirigami folding and soldering; (f) finished sample.
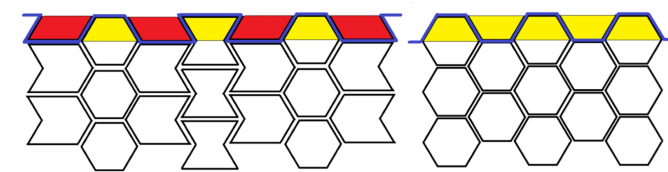

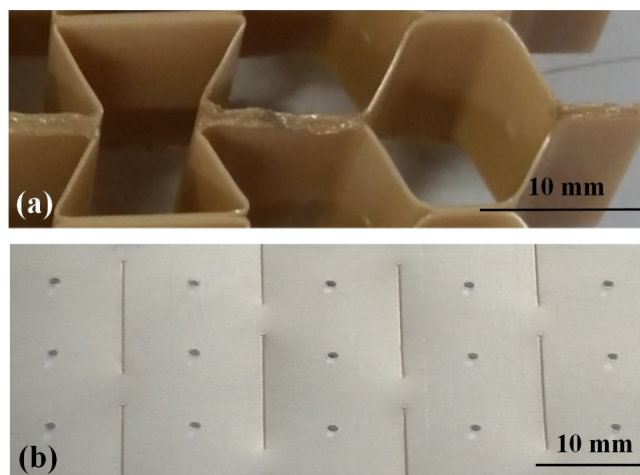Fig. 9: PEEK film (blue) around the mould bars and consequent cellular structure obtained with Kirigami folding.
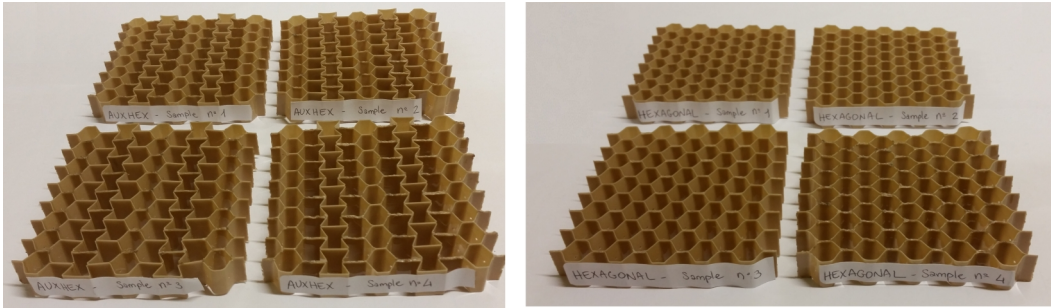

Fig. 10: Soldering details (a) and vent holes (b).

20

Fig. 11: AuxHex (Left) and hexagonal (right) samples produced and ready to be tested.
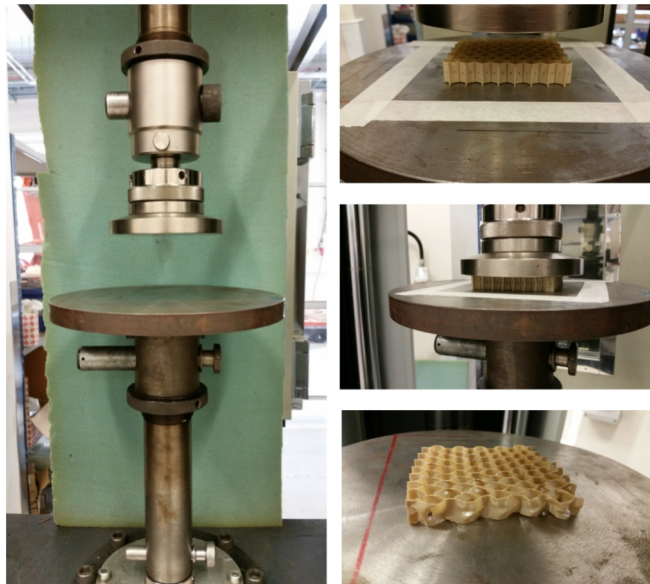

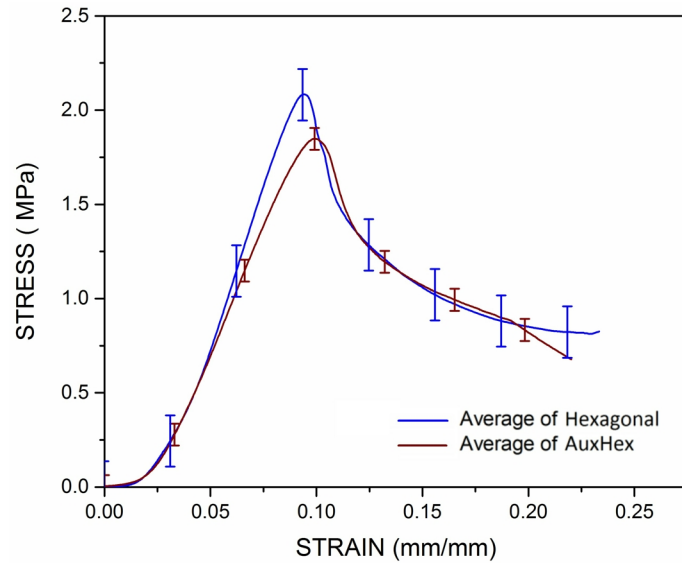Fig. 12: Mechanical testing of the specimens.

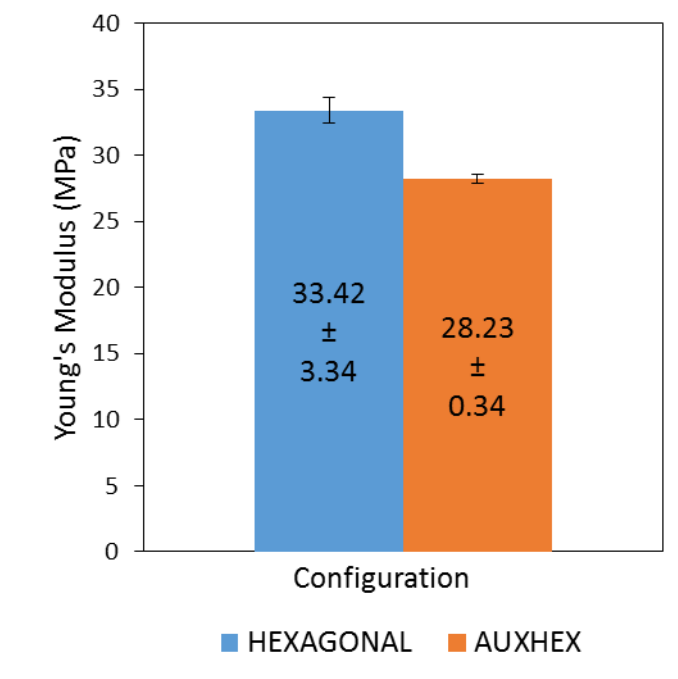Fig. 13: Ultimate compressive stress from mechanical testing.

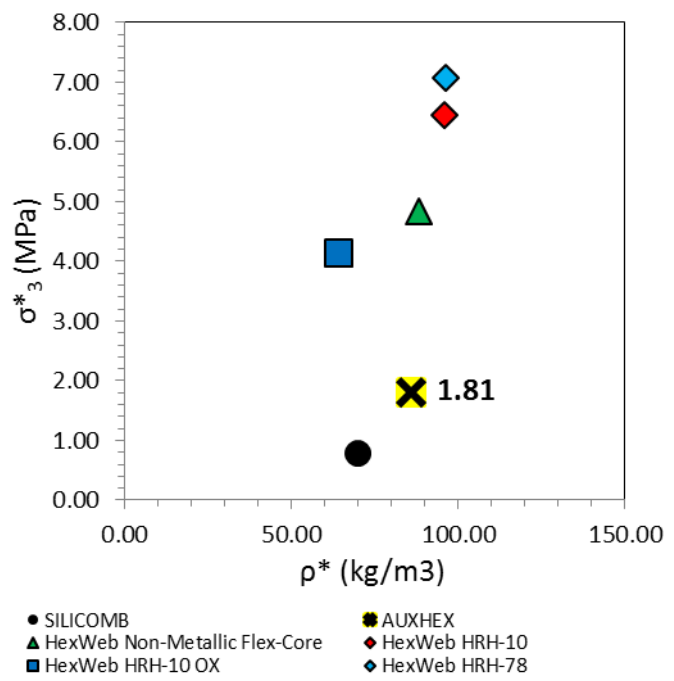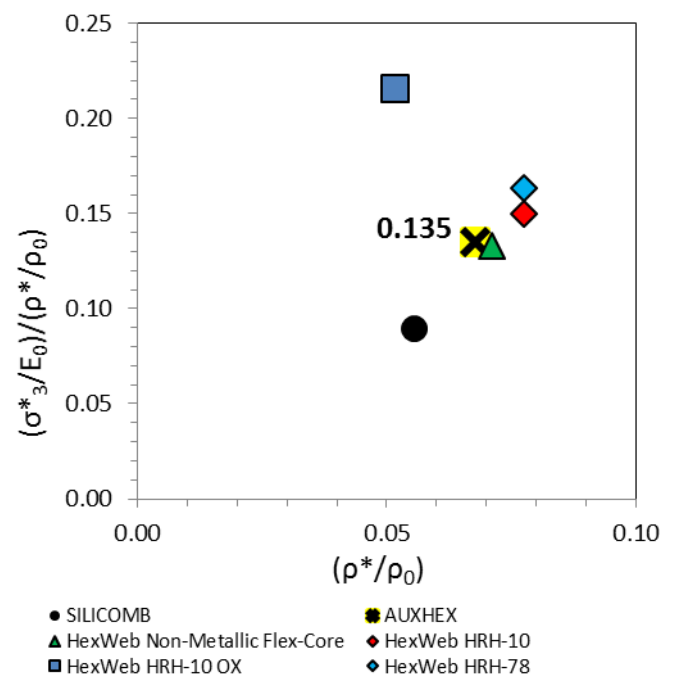Fig. 14: Young's modulus calculated from mechanical testing results.

Fig. 15: AuxHex ultimate compressive strength comparison with competitors.

σ^*_3 = Ultimate compressive strength

E_0 = Constituent Elastic modulus

ρ^* = Core density

ρ_0 = Material density

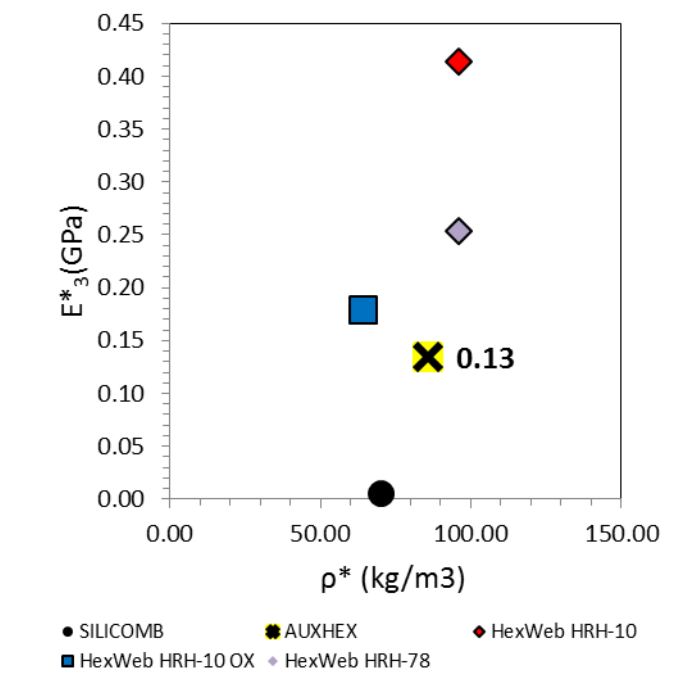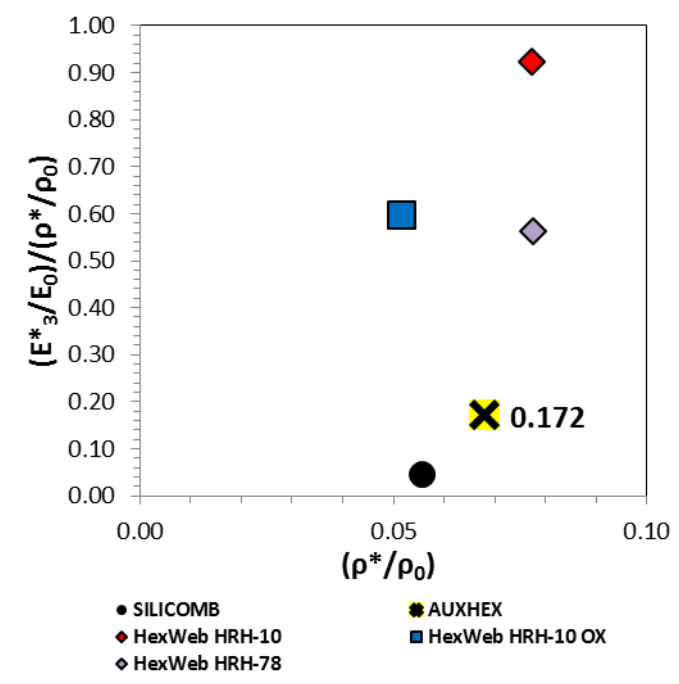Fig. 16: AuxHex normalized ultimate compressive strength comparison with competitors.

Fig. 17: AuxHex Young's modulus comparison with competitors.

E^*_3 = Core elastic modulus

E_0 = Material elastic modulus

ρ^* = Core density

ρ_0 = Material density

Fig. 18: AuxHex normalized Young's modulus comparison with competitors.

CONSTRAINT	ELASTIC COLLAPSE STRESS σ_z (MPa)	
	HEXAGONAL	AUXHEX
SS	11.012	4.434
SS/C	6.336	2.572
SS/Free	0.793	0.386
C/Free	2.325	0.917

Table 1: Elastic collapse stress considering unit cells with same boundary conditions for all walls.

CONFIGURATION	CELL TYPE	N°CELLS	SURFACE AREA (mm²)
HEXAGONAL	Hexagonal	68	27600
	(TOTAL)	(68)	(240mm x 115mm)
AUXHEX	Hexagonal	24	
	Butterfly	16	34080
	Arrow	28	(240mm x 143mm)
	(TOTAL)	(68)	

SAMPLE (average)	SURFACE AREA (mm²)	VOLUME (mm³)	WEIGHT (g)	DENSITY (Kg/m³)	RELATIVE DENSITY ρ^*/ρ
HEXAGONAL	7642.59	11467.92	8.72	76.03	0.06
AUXHEX	8418.90	126304.50	10.84	85.80	0.07

Table 2: Sample average dimensions.

CORE TYPE	PROPERTY	$\dfrac{property/E_s}{\rho^*/\rho}$
AUXHEX	Ultimate strength	0.14
	Young's Modulus	0.17
SILICOMB	Ultimate strength	0.09
	Young's Modulus	0.05

Table 3: Normalized properties for AuxHex and Silicomb configurations.

NAME	TYPE/MATERIAL
HexWeb Metallic Flex-Core	Al 5052/5056 alloy foil
HexWeb Non-Metallic Flex-Core	NOMEX aramid paper + phenolic resin
HexWeb HRH-10	Aramid fiber + phenolic resin
HexWeb HRH-10 OX (Over Expanded)	Aramid fiber + phenolic resin
HexWeb HRH-78	NOMEX paper + phenolic resin

Table 4: Commercially available competitors

References

[1] Sinapius M, Monner HP, Kintscher M, Riemenschneider J. DLR's Morphing Wing Activities within the European Network. Procedia IUTAM. 2014;10:416-26.

[2] Sofla AYN, Meguid SA, Tan KT, Yeo WK. Shape morphing of aircraft wing: Status and challenges. Materials & Design. 2010;31(3):1284-92.

[3] Chillara VSC, Headings LM, Dapino MJ. Multifunctional composites with intrinsic pressure actuation and prestress for morphing structures. Composite Structures. 2016;157:265-74.

[4] Takahashi H, Yokozeki T, Hirano Y. Development of variable camber wing with morphing leading and trailing sections using corrugated structures. Journal of Intelligent Material Systems and Structures. 2016.

[5] Costantine J, Tawk Y, Maqueda I, Sakovsky M, Olson G, Pellegrino S, et al. UHF Deployable Helical Antennas for CubeSats. IEEE Transactions on Antennas and Propagation. 2016;64(9):3752-9.

[6] Zhang Y, Yang D, Li S. An integrated control and structural design approach for mesh reflector deployable space antennas. Mechatronics. 2016;35:71-81.

[7] Arya M, Lee N, Pellegrino S. Ultralight Structures for Space Solar Power Satellites. 2016.

[8] Hogstrom K, Pellegrino S. Methods for Characterizing the Reliability of Deployable Modules for Large Optical Reflectors. 2016.

[9] Pellegrino S. Deployable Structures: Springer-Verlag Wien New York; 2001.

[10] Litteken DA. Strain Monitoring of Flexible Structures. In: Forum ST, editor. AIAA Sci Tech 20172016.

[11] Nojima T. Origami Modeling of Functional Structures based on Organic Patterns 1996.

[12] Nojima S. Development of Newly Designed Ultra-Light Core Structures. JSME International Journal. 2006;49(1).

[13] Saito K, Nojima T. Development of Light-Weight Rigid Core Panels. Journal of Solid Mechanics and Materials Engineering. 2007;1(9):1097-104.

[14] Nojima T. Modelling of folding patterns in flat membranes and cylinders by Origami. JSME, International Journal. 2002 45(1).

[15] Saito K, Tsukahara A, Okabe Y. New Deployable Structures Based on an Elastic Origami Model. Journal of Mechanical Design. 2014;137(2):021402.

[16] Saito K, Agnese F, Scarpa F. A Cellular Kirigami Morphing Wingbox Concept. Journal of Intelligent Material Systems and Structures. 2011;22(9):935-44.

[17] Neville S. Design of Shape Morphing Cellular Structures and Their Actuation Methods. ICAST2015: 26th International Conference on

Adaptive Structures and Technologies. Kobe, Japan2015

[18] Neville RM, Scarpa F, Pirrera A. Shape morphing Kirigami mechanical metamaterials. Sci Rep. 2016;6:31067.

[19] Saito K, Pellegrino S, Nojima T. Manufacture of Arbitrary Cross-Section Composite Honeycomb Cores Based on Origami Techniques. Journal of Mechanical Design. 2014;136(5):051011.

[20] S. Zirbel BT. Sola Power, Origami-Style. 2014. p. NASA, JPL Website.

[21] A. Lamoureux KL, M. Shlian, S.R. Forrest, M. Shtein. Dynamic Kirigami structures for integrated solar tracking. Nature Communications. 2015:6.

[22] Shyu TC, Damasceno PF, Dodd PM, Lamoureux A, Xu L, Shlian M, et al. A kirigami approach to engineering elasticity in nanocomposites through patterned defects. Nat Mater. 2015;14(8):785-9.

[23] Blees MK, Barnard AW, Rose PA, Roberts SP, McGill KL, Huang PY, et al. Graphene kirigami. Nature. 2015;524(7564):204-7.

[24] Hou Y, Neville R, Scarpa F, Remillat C, Gu B, Ruzzene M. Graded conventional-auxetic Kirigami sandwich structures: Flatwise compression and edgewise loading. Composites Part B: Engineering. 2014;59:33-42.

[25] Grima JN, Oliveri L, Attard D, Ellul B, Gatt R, Cicala G, et al. Hexagonal Honeycombs with Zero Poisson's Ratios and Enhanced Stiffness. Advanced Engineering Materials. 2010;12(9):855-62.

[26] Lorna J. Gibson MFA. Cellular Solids. Second Edition ed: Cambridge University Press; 1997.

[27] Warren C. Young RGB. Roark's Formulas for Stress and Strain.

[28] Victrex. APTIV film series 2000-250. In: Victrex, editor.2015.

[29] Chen Y, Scarpa F, Remillat C, Farrow I, Liu Y, Leng J. Curved Kirigami SILICOMB cellular structures with zero Poisson's ratio for large deformations and morphing. Journal of Intelligent Material Systems and Structures. 2013;25(6):731-43.

[30] Neville RM, Monti A, Hazra K, Scarpa F, Remillat C, Farrow IR. Transverse stiffness and strength of Kirigami zero-ν PEEK honeycombs. Composite Structures. 2014;114:30-40.

[31] International A. Flatwise Test Method for Flatwise Compressive Proeprties of Sandwich Cores.

[32] Lira C, Scarpa F, Tai YH, Yates JR. Transverse shear modulus of SILICOMB cellular structures. Composites Science and Technology. 2011;71(9):1236-41.

[33] Vandenbrink DJ. Post-bucking response of isotropic and laminated composite square plates with circular holes. FInite Elements in Analysis and Design. 1987;3(3):165-74.

[34] Onck PR. Scale Effects in Cellular Metals. Materials Research Society. 2003;28(04):279-83.

[35] C.C. Foo GBC, L.K. Seah. Mechanical properties of Nomex material and Nomex honeycomb structure. Composite Structures. 2007;80(4):588-94.

[36] J. Zhabg MFA. The out-of-plane properties of Honeycombs. Int J Mech Sci. 1992;34(6):475-89.